

## Novel biologically active polyurea derivatives and its TiO<sub>2</sub>-doped nanocomposites

Mahmoud A. Hussein<sup>a,b</sup>, Khalid A. Alamry<sup>a</sup>, Samar J Almeahdi<sup>a</sup>, M.A. Elfaky<sup>c</sup>, H. Džudžević-Čančar<sup>d</sup>, Abdullah M. Asiri<sup>a,e</sup> and Mostafa A. Hussien<sup>a,f</sup>

<sup>a</sup>Department of Chemistry, Faculty of Science, King Abdulaziz University, Jeddah, Saudi Arabia; <sup>b</sup>Polymer Chemistry Lab., Chemistry Department, Faculty of Science, Assiut University, Assiut, Egypt; <sup>c</sup>Faculty of Pharmacy, Natural Products and Alternative Medicine Department, King Abdulaziz University, Jeddah, Saudi Arabia; <sup>d</sup>Department of Natural Science in Pharmacy, Faculty of Pharmacy, University of Sarajevo, Sarajevo, Bosnia-Herzegovina; <sup>e</sup>Center of Excellence for Advanced Materials Research, King Abdulaziz University, Jeddah, Saudi Arabia; <sup>f</sup>Department of Chemistry, Faculty of Science, Port Said University, Port Said, Egypt

### ABSTRACT

A new series of polyurea derivatives and its nanocomposites were synthesised by the solution polycondensation method through the interaction between 4(2-aminothiazol-4-ylbenzylidene)-4-(tert-butyl) cyclohexanone and diisocyanate compound in pyridine. The PU<sub>1-3</sub> structure was confirmed using Fourier transform-infrared (FTIR) spectroscopy and characterised by solubility, viscometry, gel permeation chromatography (GPC), and X-ray diffraction (XRD) analysis. In addition, PU<sub>1-3</sub> was evaluated by TGA. Polyurea-TiO<sub>2</sub> nanocomposites were synthesised using the same technique as that of PU<sub>1-3</sub> by adding TiO<sub>2</sub> as a nanofiller. The thermal properties of PU<sub>2</sub>TiO<sub>2</sub>a-d were evaluated by TGA. Moreover, the morphological properties of a selected sample were examined by SEM and TEM. In addition, PU<sub>1-3</sub> and PU<sub>2</sub>TiO<sub>2</sub>a-d were examined for antimicrobial activity against certain bacteria and fungi. The PU<sub>1-3</sub> showed antibacterial activity against some of the tested bacteria and fungi, as did PU<sub>2</sub>TiO<sub>2</sub>a-d, which increased with the increase in TiO<sub>2</sub> content. Furthermore, molecular docking studies were displayed against all PU<sub>1-3</sub> derivatives against two types of proteins. The results show that the increase in the strength of  $\pi$ -H interactions and H-donors contributed to improved binding of PU<sub>2</sub> compared to PU<sub>1</sub> and PU<sub>3</sub>. The docking of 1KZN against the tested polymers suggests an increase in the docking score of PU<sub>2</sub>, then PU<sub>1</sub>, and PU<sub>3</sub>, which is in agreement with the antibacterial study.

### ARTICLE HISTORY

Received 5 February 2020  
Accepted 5 May 2020

### KEYWORDS


Polyurea derivatives;  
nanocomposites; TiO<sub>2</sub>;  
antibacterial activity;  
molecular docking

## 1. Introduction

Polyurea derivatives are important polymers obtained by the interaction between a diisocyanate and an amine. Polyurea is an extremely rough material and exhibits high hardness and good chemical resistance, which enable it to have many applications, for example, in corrosion protection and coating systems [1]. Many efforts to synthesise a new class of thermally stable polyurea to achieve different properties have been reported, such as phosphorus-containing heterocyclic polyurea [2–5]. Heterocyclic-based PU derivatives or by another wards, metal-containing PU with an ionic link in the main chain was synthesised and received great attention [6,7]; meanwhile, the introduction of a metal into heterocyclic polyurea, to achieve a versatile number of variable properties, has been studied, and the polymer chain was reported as a possible cause for their increased thermal stability [2,3,5,8].

Several techniques have been used to synthesise polyurea, but the most effective technique is to react diamine with diisocyanate. This reaction is a step-growth addition reaction of amine across the carbon-nitrogen double bond, and there is no by-product. The essential components for a compound to be an efficient inhibitor are [9]: (i) it should be chemisorbed onto the metal surface, (ii) it should form a defect-free compact barrier film, (iii) it should be polymeric or polymerise in situ on the metal, and (iv) the barrier thus formed should increase the inner layer thickness. Compounds containing nitrogen, sulfur, and oxygen have been established as good inhibitors for iron in acidic media [9]. The  $\pi$  bonds inorganic compounds are found in corrosion inhibition of steel by being adsorbed through electron sharing on the electrode surface [10]. The presence of functional groups, for example, NH<sub>2</sub>, N = N, CHO, and R-OH, in the inhibitor molecule [11], steric factors, aromaticity, and electron

**CONTACT** Mahmoud A. Hussein  [mahusse74@yahoo.com](mailto:mahusse74@yahoo.com)

 Supplemental data for this article can be accessed [here](#).

© 2020 The Author(s). Published by Informa UK Limited, trading as Taylor & Francis Group.

This is an Open Access article distributed under the terms of the Creative Commons Attribution License (<http://creativecommons.org/licenses/by/4.0/>), which permits unrestricted use, distribution, and reproduction in any medium, provided the original work is properly cited.

density of the donor atoms are found to influence the adsorption of the inhibitor molecule over the corroding electrode surface.

Recently, some polymers [12–14] have received intensive attention because of their wide application range. This work continues our previous studies regarding the preparation of various types of organic polymers and/or polymer nanocomposite materials having interesting properties and thus can find widespread applications in different fields of study [15–31].

According to our best of knowledge, there are no previous reports for PU derivatives reinforced by TiO<sub>2</sub> nanoparticles in the form of nanocomposites. A general understanding which describes the role of reinforced inorganic material throughout the nanocomposite formation and about how organic polymer interacts with inorganic particles in the nanoscale to form a composite material has been reported in the literature [32–36]. In this study, we address the synthesis and characterization of new polyurea derivatives containing diarylidene cyclohexanone moiety in the polymer and prepare the polymer nanocomposite using TiO<sub>2</sub> nanoparticles. TiO<sub>2</sub> is a commonly used material because it is inexpensive, is non-toxic, has a high refractive index, can be used as a broadband UV filter, is chemically inert, exhibits biological activity against bacteria via photo-irradiation, is corrosion-resistant, and has high rigidity [37].

The main goal of the present work is to synthesize a new series of polyurea derivatives and its related TiO<sub>2</sub> nanocomposites. The prepared materials are characterized by investigating their crystallinity, thermal stability, solubility, viscometry, morphology. Moreover, the GPC measurement is also used to determine the molecular weight of the synthesised polyurea. Finally, investigate their antimicrobial properties as well as molecular docking studies.

## 2. Experimental method

### 2.1. Measurements

IR spectra were recorded on an IR-470, infrared spectrophotometer. The <sup>1</sup>H NMR spectra were obtained on GNM-LA (400 MHz) spectrophotometer at room temperature in CDCl<sub>3</sub> using TMS as a reference. Inherent viscosities of polyurea solutions were measured in dimethyl sulfoxide (DMSO) at 30°C using an Ubbelohde suspended-level viscometer. The polymer solubility was tested for powdery samples at room temperature under the same conditions with different

solvents: formic acid, chloroform (CHCl<sub>3</sub>), dichloromethane (CH<sub>2</sub>Cl<sub>2</sub>), benzene, dimethylformamide (DMF), sulfuric acid, and DMSO. The molecular weight of polyurea was evaluated by GPC using an Agilent-GPC from Agilent Technologies in Germany. The refractive index detector was G-1362A with 100–104–105 Å Altrastyrigel columns connected in series. The eluent used was DMF at a flow rate of 1 mL/min and in the presence of PS as a reference polymer. The GPC apparatus was run under the following conditions: flow rate = 2.000 mL/min, injection volume = 100.000 µL, and sample concentration = 1.000 g/L. X-ray diffraction (XRD) measurements of polyurea derivatives and polyurea–TiO<sub>2</sub> nanocomposites with different TiO<sub>2</sub> nanoparticle contents (2%, 5%, 10%, and 20%) were recorded on an XRD D8 Discovery model manufactured by the Bruker Company in Germany. XRD measurements were conducted at 40 kV and 40 mA over a scanning range from 5° to 90° at a scan speed/duration time of 4.0000 deg/min. Thermal analysis was performed by thermogravimetric analysis (TGA) using the Shimadzu-D50 thermal analyser model manufactured by the Shimadzu Company (Japan). The rate of temperature increase was 10°/min, holding temperature 800°C using platinum cell and air atmosphere. Transmission electronic microscopy (TEM) measurements were recorded using an EM-2100 High-Resolution model at 25X magnification and 200 kV. TEM images were taken only for polyurea–TiO<sub>2</sub> nanocomposites with 20% TiO<sub>2</sub> nanoparticles. SEM images were taken on a Jol 2000 (Japan) model for polyurea–TiO<sub>2</sub> nanocomposites with 2% and 20% TiO<sub>2</sub> nanoparticles.

### 2.2. Reagents and solvents

TiO<sub>2</sub> nanoparticles with a size of <50 nm and 4-tert-butylcyclohexanone (Merck, Germany) were used as purchased. Chloroacetyl chloride and thiourea (Merck, Germany) were used as received. Anhydrous aluminium chloride (Aldrich, Germany) was used as purchased, while hexamethylene diisocyanate, 4,4'-diphenylmethane diisocyanate, 1,4-phenylenediisocyanate (all from Aldrich, 97%), and pyridine (Merck, Germany) were dried using sodium hydroxide pellets for three days. Methanol (absolute, 99.8%), ethanol (absolute, 99.9%), and acetone (Merck, Germany) were used as purchased. Carbon disulfide (Merck, Germany) was dried overnight by calcium chloride, and then distilled under reduced pressure.

## 2.3. Monomer synthesis

### 2.3.1. 2,6-bis-(benzylidene)-4-(tert-butyl)cyclohexanone (M1)

New monomer, namely, 2,6-bis-(benzylidene)-4-(tert-butyl)cyclohexanone (M1), was synthesised according to the following general procedure. A mixture of 0.02 moles of benzaldehyde and 0.01 mole of 4-(tert-butyl) cyclohexanone in warm ethanol (10 mL of ethanol per gram of the mixture) was prepared. To this was added 10% potassium hydroxide solution dropwise until a yellow solid precipitate was formed. The precipitate was collected, and the remaining solution was stirred for 3–4 h. The precipitate was collected by filtration and then washed with cold water and recrystallized from ethanol, as shown in Figure 1. The FTIR spectra of the monomer showed the absorption bands at  $2959\text{ cm}^{-1}$  (CH aliphatic),  $1661\text{ cm}^{-1}$  (C = O of cyclohexanone), and  $1604\text{ cm}^{-1}$  (C = C). Additional details are found in Figure S1.<sup>1</sup> HNMR spectrum of 2,6-dibenzylidene-4-tert-butyl-cyclohexanone (CDCl<sub>3</sub>)

showed peaks at  $\delta = 1.26$  (s, 9 H, 3CH<sub>3</sub>), 2.4–2.62 (m, 1 H, CH), 3.15–3.19 (m, 4 H, 2CH<sub>2</sub> of cyclohexanone), and 7.25–7.78 (m, 12 H, 2CH = C & 10Ar-H). Additional details can be found in Figure S4. <sup>13</sup>CNMR (CDCl<sub>3</sub>):  $\delta = 27.29, 32.58, 44.44, 128.84, 128.56, 130.36, 136.06, 136.19, 136.87, 190.65$ . Additional details can be found in Figure S8.

### 2.3.2. Bis (4-chloroacetylbenzylidene)-4-(tert-butyl)cyclohexanone (M2)

In a conical flask, 0.02 mole of M1 and 0.04 mole of chloroacetyl chloride were added and the mixture dissolved in 80 mL of carbon disulfide. Then, anhydrous aluminium chloride (0.08 mole) was added dropwise. The mixture was stirred in an ice bath for 6 h, then the carbon disulfide was evaporated and the residue poured into cold hydrochloric acid. The yellow-precipitated product was collected by filtration, washed with water, and recrystallized from an appropriate solvent as shown in Figure 2. The IR spectra of this monomer showed absorption

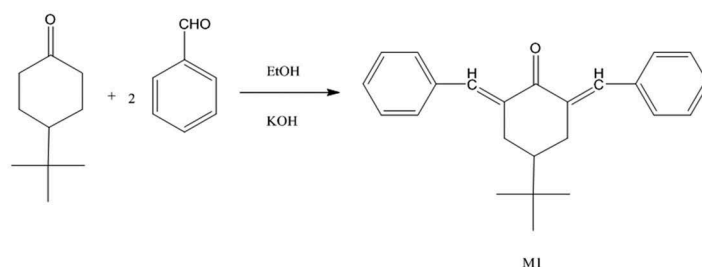


Figure 1. Synthesis of 2,6-bis-(benzylidene)-4-(tert-butyl)cyclohexanone monomer.

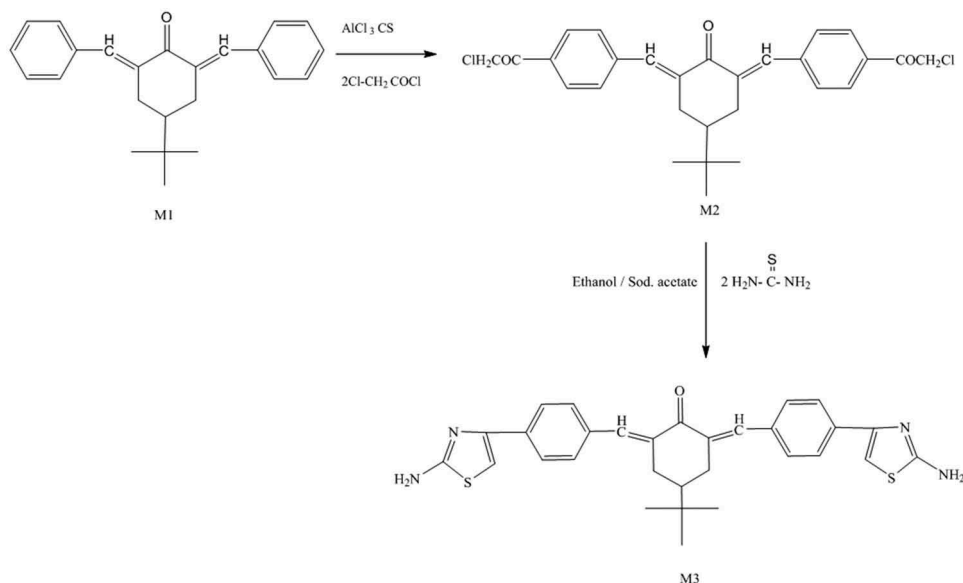


Figure 2. Synthesis of diarylidene cyclohexanone monomers M2 and M3.

bands at  $1735\text{ cm}^{-1}$  (C = O of chloroacetyl group), with the original absorption bands of  $1660\text{ cm}^{-1}$  (C = O of cyclohexanone) and  $1602\text{ cm}^{-1}$  (C = C) (further information is in Figure S2).  $^1\text{H NMR}$  spectra (in  $\text{CDCl}_3$ ) showed peaks at  $\delta = 6.82\text{--}7.85$  (m, 10 H, 2CH = C & 8 H of aromatic), 4.15 (s, 4 H of  $\text{CH}_2$  chloroacetyl), 3.14–3.18 (m, 4 H, 2 $\text{CH}_2$  of cyclohexanone), 2.41–2.64 (m, 1H, CH), and 0.97 (s, 9 H, 3 $\text{CH}_3$ ). Additional details are in figure S5.  $^{13}\text{C NMR}$  ( $\text{CDCl}_3$ ):  $\delta$  27.29, 29.30, 29.53, 32.58, 44.44, 53.85, 69.53, 128.47, 128.56, 130.31, 136.18, 136.87, 190.66, 210.79. Additional details can be found in Figure S9.

### 2.3.3. Bis(2-aminothiazol-4-ylbenzylidene)-4-(tert-butyl) cyclohexanone (M3)

A mixture of 0.02 moles of M2 and 0.04 moles of thiourea was dissolved in 40 mL of ethanol and then stirred under reflux for 5 h. The clear solution was poured into cold sodium acetate solution (10%; 25 mL), and the precipitate formed was collected filtered, and re-crystallized using a proper solvent, as shown in Figure 2. The IR spectra showed absorption bands at  $3370\text{--}3333\text{ cm}^{-1}$ , attributed to the primary amino group, and at  $1630\text{ cm}^{-1}$  (C = N), together with the original bands of the parent

monomer at  $1660\text{ cm}^{-1}$  (C = O of cyclohexanone),  $1604\text{ cm}^{-1}$  (C = C), and phenylene at  $1580\text{ cm}^{-1}$  (additional information is in Figure S3).  $^1\text{H NMR}$  spectra (in  $\text{CDCl}_3$ ) showed peaks at  $\delta = 6.80\text{--}7.84$  [m, 12 H, 8 H of aromatic and 2 H(CH = C) and 2 H(CH–S)], 5.30 (s, 4 H of  $\text{NH}_2$  exchangeable with  $\text{D}_2\text{O}$ ), 3.18–3.20 (m, 4 H 2 $\text{CH}_2$  of cyclohexanone), 2.47–2.64 (m, 1H, CH), and 0.977 (s, 9 H of butyl). More information can be found in Figure S6 and Figure S7 before and after adding the  $\text{D}_2\text{O}$  respectively.  $^{13}\text{C NMR}$  ( $\text{CDCl}_3$ ):  $\delta$  26.90, 27.30, 27.97, 29.34, 29.84, 29.52, 29.68, 29.71, 32.56, 40.95, 44.38, 103.79, 125.99, 128.48, 128.57, 128.59, 130.33, 130.84, 134.71, 135.33, 136.03, 136.07, 136.20, 136.67, 136.84, 136.92, 150.64, 167.60, 190.62. Additional details can be found in Figure S10.

### 2.4. Polymerization process

In a three-necked flask equipped with a condenser and dry nitrogen inlet and outlet, a mixture of 0.002 moles of M3 was dissolved in 30–40 mL of dry pyridine. The different aromatic and aliphatic diisocyanates (0.002 moles) dissolved in 15 mL of dry pyridine, were added in a dropwise manner while stirring. After complete addition of the diisocyanate,

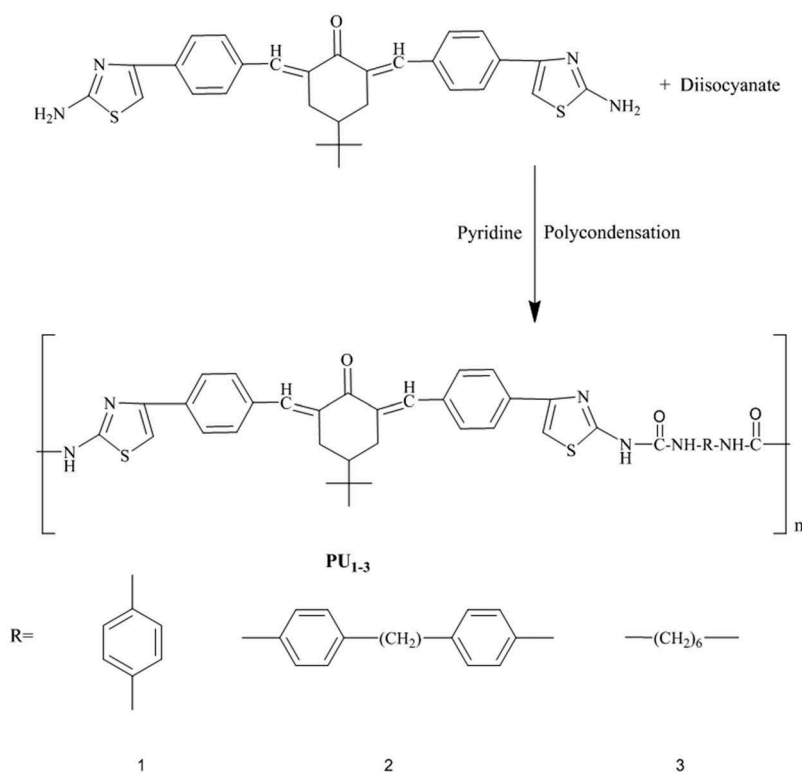


Figure 3. Synthesis of polyurea derivatives  $\text{PU}_1$ ,  $\text{PU}_2$ , and  $\text{PU}_3$ .

the reaction mixture was heated under reflux for 15 h and cooled to room temperature. Subsequently, the mixture was poured into ice water, forming a white–brownish precipitate (PU<sub>1</sub>, PU<sub>2</sub>, and PU<sub>3</sub>) as shown in Figure 3. Then, the solid polymers were separated out, filtered, and washed with water. The IR spectra of the polymers showed absorption bands at 3340 cm<sup>-1</sup> (NH of urea derivative) and 1680 cm<sup>-1</sup> (C = O of urea derivative).

### 2.5. Polyurea-based TiO<sub>2</sub> nanocomposites fabrication process

The PU<sub>2</sub>TiO<sub>2</sub>a–d were synthesised by adding TiO<sub>2</sub> nanoparticles in different contents (2%, 5%, 10%, 20%) to the solvent (dry pyridine). The mixture was poured into ice water, to remove any excess of pyridine. The same procedure was repeated to synthesise polyurea (see previous section). The polymer data are shown in Table 1. The IR spectra of PU<sub>2</sub>TiO<sub>2</sub>a–d show absorption bands at 3330 cm<sup>-1</sup>

(NH of urea derivative) and 1660 cm<sup>-1</sup> (C = O of urea derivative).

### 2.6 Antimicrobial activity

Antimicrobial activity was tested for the new synthesised polyurea and polyurea–TiO<sub>2</sub> nanocomposites by using the agar diffusion method with different bacterial species and fungi: gram-positive bacteria strains (*Bacillus subtilis* and *Staphylococcus aureus*) and gram-negative bacteria strains (*Pseudomonas aeruginosa* and *Escherichia coli*), and fungus (*Candida albicans*). All organisms were kept in the microbiology lab at King Abdulaziz University in Jeddah, Saudi Arabia. The technique used to determine the antimicrobial effect for the new polymer has been described previously [38]. In brief, a 90-mm Petri dish was filled with 25 mL of Muller–Hinton agar; then, 200 μL bacterial cultures were autoclaved for 20 min and were spread on the agar plate surfaces by using sterile swabs. Next, 50 μL of the polymer was added to the agar plates and incubated at 37°C for 24 h. The size of the growth inhibition zone was measured and determined as shown in Table 5.

**Table 1.** Polymers its related TiO<sub>2</sub> doped nanocomposites symbols and codes.

Code	TiO <sub>2</sub> nanoparticles (%)	TiO <sub>2</sub> nanoparticles wt. (g)
PU <sub>1</sub>	0	0
PU <sub>2</sub>	0	0
PU <sub>3</sub>	0	0
PU <sub>2</sub> TiO <sub>2</sub> a	2%	0.036
PU <sub>2</sub> TiO <sub>2</sub> b	5%	0.071
PU <sub>2</sub> TiO <sub>2</sub> c	10%	0.18
PU <sub>2</sub> TiO <sub>2</sub> d	20%	0.36

### 2.7. Molecular docking method

All docking studies were performed using the MOE program. Structural optimization of compounds 3a and 3b was performed using ChemBioDraw ultra, and their 3D structures were constructed using ChemBio3D ultra 13.0 software Molecular Modelling

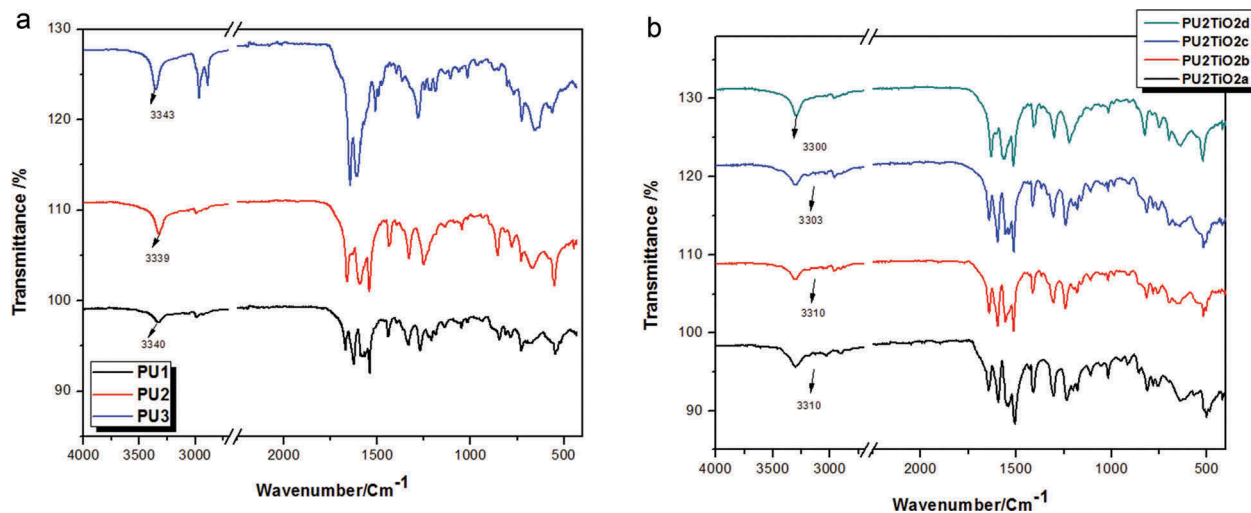


**Figure 4.** (a) FTIR spectra of polyurea derivatives PU<sub>1</sub>, PU<sub>2</sub>, and PU<sub>3</sub>. (b) FTIR spectra of Polyurea–TiO<sub>2</sub> nanocomposites PU<sub>2</sub>TiO<sub>2</sub>a–d.



and Analysis, Cambridge Soft Corporation; they were then energetically minimised using MOPAC and saved as MDL Mol File (\*.mol). The target crystal structures were retrieved from the Protein Data Bank (<http://www.rcsb.org/pdb/>). All bound water ligands and cofactors were removed from the protein, and the water molecules around the duplex were also removed before adding the hydrogen atoms. The parameters and charges were assigned with the MMFF94x force field. After alpha-site spheres were generated using the site finder module of MOE, the structural model of complexes was docked on the surface of the interior of the minor groove using the DOCK module of MOE [39–41]. All calculations

were performed on an Intel(R) core (TM)i7, 3.8 GHz-based machine with MS Windows 10 as the operating system. The Dock scoring in MOE software was done utilizing the London dG scoring function and has been upgraded using two unrelated refinement methods. In addition, auto rotatable bonds were allowed; the ten best binding poses were directed and analysed to achieve the best score. To compare the docking poses to the ligand in the co-crystallised structure and to obtain the RMSD of the docking pose, the database browser was used. To rank the binding affinity of the synthesised compounds to the protein molecule, the binding-free energy and hydrogen bonds between the compounds and amino acid in the receptor were used. Evaluation of the hydrogen bonds was done by measuring the hydrogen bond length, which did not exceed 3.5 Å. In addition, RMSD of the compound position compared to the docking pose was used in ranking. Both RMSD and the mode of interaction of the native ligand within the structure of the receptor were used in the standard-docked model.

**Table 2.** Solubility characteristics of PU<sub>1</sub>, PU<sub>2</sub>, and PU<sub>3</sub>.

Polymer Code	DMF	HCOOH	CHCl <sub>3</sub>	CH <sub>2</sub> Cl <sub>2</sub>	DMSO	H <sub>2</sub> SO <sub>4</sub>	Benzene
PU <sub>1</sub>	+	+	+	+–	+	+	+–
PU <sub>2</sub>	+	+	+	+–	+	+	+–
PU <sub>3</sub>	+	+	+	+–	+	+	+–

+Soluble at room temperature.

+–Partially soluble.

–Insoluble.

**Table 3.** Inherent viscosities and GPC results for PU<sub>1</sub>, PU<sub>2</sub>, and PU<sub>3</sub>.

Code	M. Formula	GPC data				$\eta_{inh}$ (dL/g)
		<sup>a</sup> M <sub>w</sub>	<sup>b</sup> M <sub>n</sub>	<sup>c</sup> P <sub>w</sub>	DPI	
PU <sub>1</sub>	(C <sub>38</sub> H <sub>36</sub> N <sub>6</sub> O <sub>3</sub> S <sub>2</sub> ) <sub>n</sub>	38,863.22	35,538.32	~ 56	1.09	0.93
PU <sub>2</sub>	(C <sub>45</sub> H <sub>42</sub> N <sub>6</sub> O <sub>3</sub> S <sub>2</sub> ) <sub>n</sub>	42,678.09	37,998.56	~ 55	1.12	0.97
PU <sub>3</sub>	(C <sub>38</sub> H <sub>42</sub> N <sub>6</sub> O <sub>3</sub> S <sub>2</sub> ) <sub>n</sub>	39,945.45	34,708.21	~ 58	1.15	1.06

<sup>a</sup>Weight-average molecular weight

<sup>b</sup>Number-average molecular weight

<sup>c</sup>Average number of repeating units

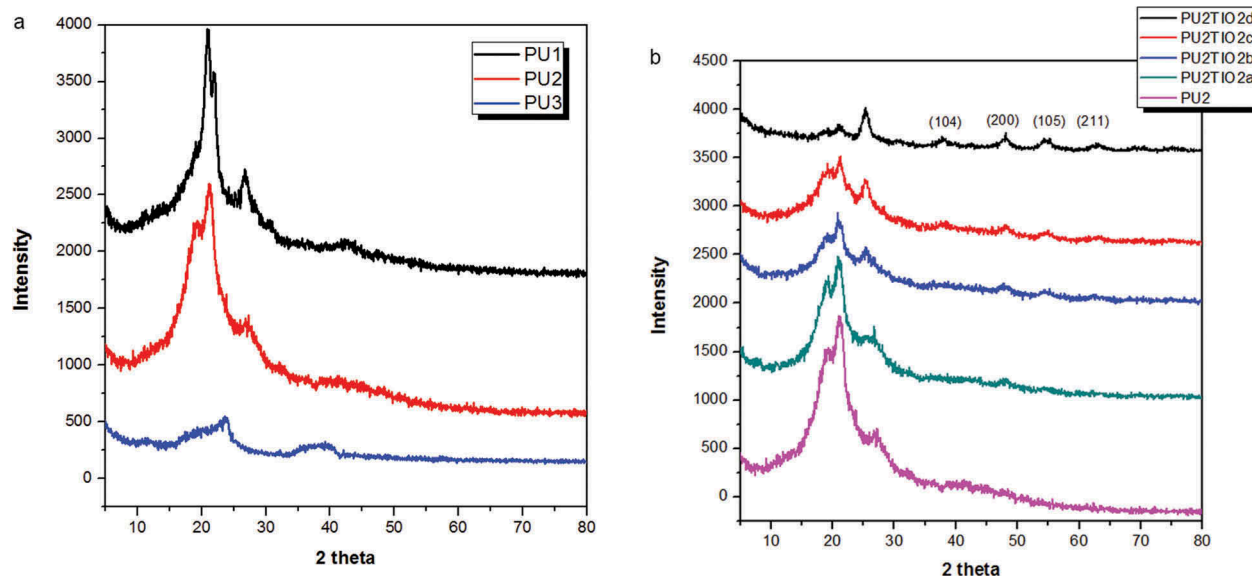


**Figure 5.** (a) X-ray diffraction patterns of PU<sub>1</sub>, PU<sub>2</sub>, PU<sub>3</sub>. (b) X-ray diffraction patterns of Polyurea-TiO<sub>2</sub> nanocomposites PU<sub>2</sub>TiO<sub>2</sub>a-d.

### 3. Results and discussion

Three new series of polyurea derivatives containing diacylidene-cyclohexanone moiety and its related TiO<sub>2</sub>-doped nanocomposites with different ratios (2%, 5%, 10%, 20%) were synthesised using *in situ* polycondensation methods. The new polymers and their nanocomposites were characterised by common characterization techniques. In addition, the biological screening for all the products has been studied. Furthermore, the molecular docking studies of PU<sub>1-3</sub> derivatives were also displayed against '5FSA' and '1KZN' proteins.

#### 3.1. Chemistry and characterization tools

M1 was synthesised using potassium hydroxide as catalysed in the mixture of 0.02 mol benzaldehyde and 0.01 mol 4-(tert-butyl)cyclohexanone in ethanol, as shown in Figure 1. The monomer structure was confirmed by FTIR and <sup>1</sup>H NMR as presented in the experimental section. M2 was synthesised by the interaction between M1 and chloroacetyl chloride in carbon disulfide using anhydrous aluminium chloride via the Friedel–Crafts reaction as shown in Figure 2. The monomer structure was confirmed by FTIR and <sup>1</sup>H NMR as presented in the experimental section. Finally, M3 was synthesised through the interaction between M2 and thiourea in absolute ethanol then stirred under reflux and poured onto sodium acetate as shown in Figure 2. The monomer structure was confirmed by FTIR and <sup>1</sup>H NMR as presented in the experimental section. Subsequently, a new series of polyurea derivatives PU<sub>1</sub>, PU<sub>2</sub>, and PU<sub>3</sub> was synthesised using the solution polycondensation procedure [42] through the interaction of M3 with diisocyanate compounds in pyridine as presented in Figure 3. The IR spectra of the polymers showed absorption bands at 3340 cm<sup>-1</sup> (NH of urea derivative) and 1680 cm<sup>-1</sup> (C = O of urea derivative), as shown in Figure 4(a).

The new polymers were characterised by solubility, viscosity, and GPC molecular weight determination as follows. The solubility of polyurea derivatives PU<sub>1</sub>, PU<sub>2</sub>, and PU<sub>3</sub> was examined at room temperature using many solvents including formic acid, CHCl<sub>3</sub>, CH<sub>2</sub>Cl<sub>2</sub>, benzene, DMF, concentrated sulfuric acid A5% (w = v), and DMSO. All solutions were prepared under the same conditions, and the polyurea derivatives were soluble in concentrated H<sub>2</sub>SO<sub>4</sub>, giving a red colour. In addition, they were soluble in polar aprotic solvents like DMSO and DMF, formic acid, and CHCl<sub>3</sub>. However, they were only partially soluble in other solvents like methylene chloride and benzene. Table 2 presents the solubility character for the synthesized PU derivative in different solvents.

The inherent viscosities were determined for PU<sub>1</sub>, PU<sub>2</sub>, and PU<sub>3</sub> in DMSO at 30°C with an Ubbelohde suspended-level viscometer. The value is defined as

$$\eta_{inh} = 2.3 \left[ \log \eta / \eta_o \right].$$

Solution concentrations were 0.5 g/100 mL and the viscosity ratio is  $\eta/\eta_o$ . Table 3 shows the viscosity value of PU<sub>1</sub>, PU<sub>2</sub>, and PU<sub>3</sub>. All polymers show viscosity values in the same range due to their very near M. Wt. values. This observation has been confirmed by the GPC measurement. Additionally, it shows that PU<sub>1</sub> had a low viscosity (0.93 dl/g) among PU<sub>1-3</sub>. The inherent viscosity ( $\eta_{inh}$ ) values for polyurea derivatives were different for each derivative, which may result in small differences in their molecular weights.

The chromatographs have different techniques used to determine the molecular weight of polymers such as column chromatography, paper chromatography, high-performance liquid chromatography (HPLC), and GPC or by other ways size exclusion chromatography (SEC) [43–45]. These different techniques pass the solution for the tested sample through a medium

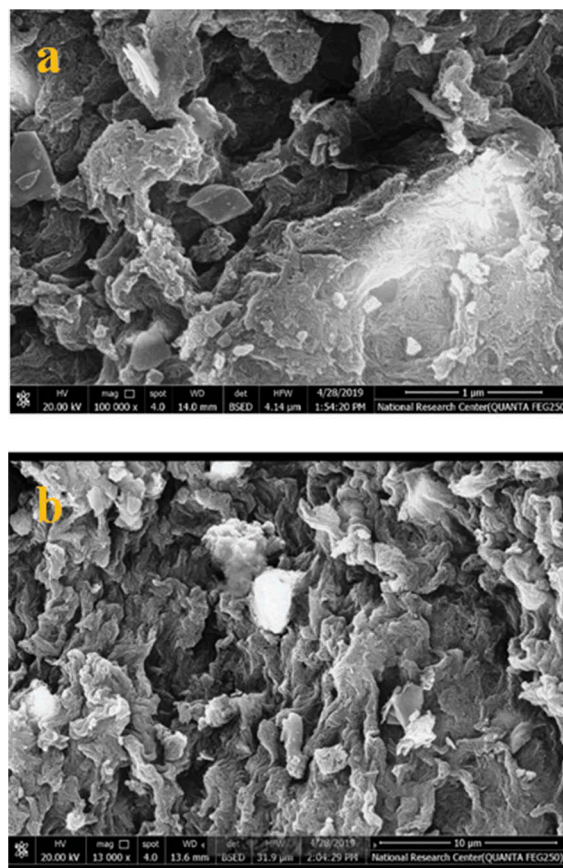


Figure 6. SEM images of PU<sub>2</sub>TiO<sub>2</sub>b at higher and lower magnifications, respectively: (a) X = 100,000, (b) X = 13,000.

that selectively absorbs the different components in the tested sample solution. GPC is extensively used for molecular weight determination. The value of the molecular weight was computed using a computer

program. The value of average number, weight-average molecular weights, and polydispersity index (Mn, Mw, and PDI) of polyurea were determined and their data are presented in Table 3.

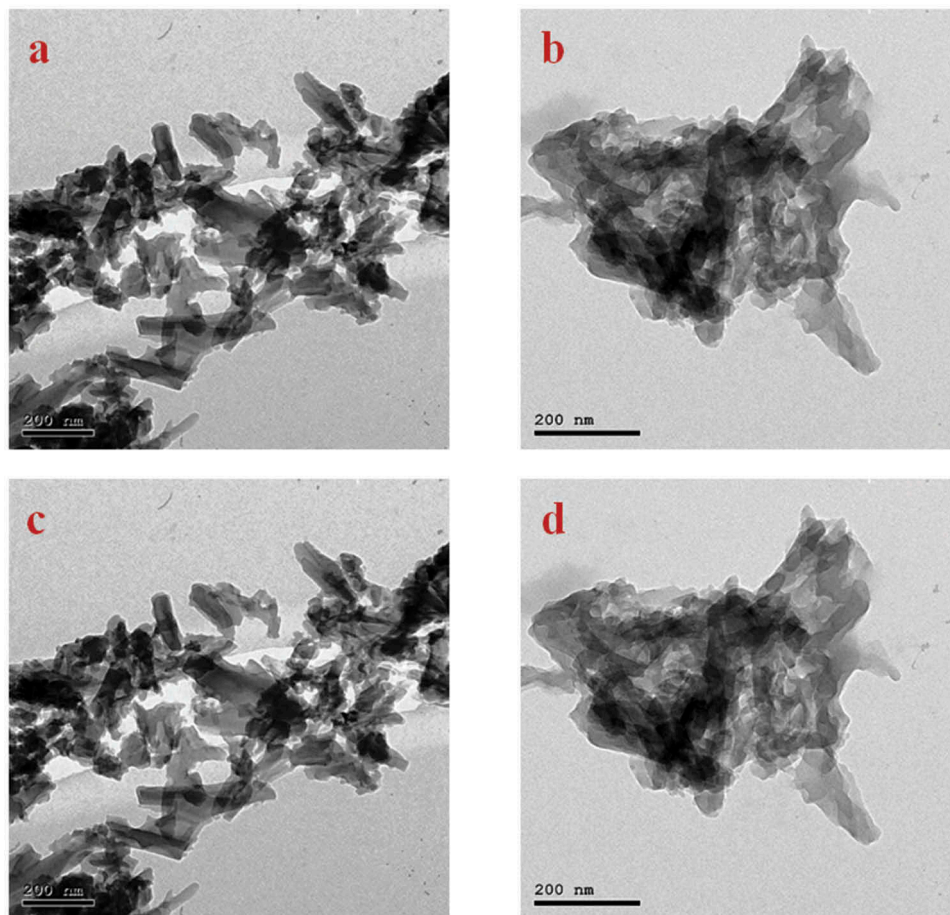


Figure 7. TEM images of  $\text{PU}_2\text{TiO}_2\text{d}$  nanocomposite.

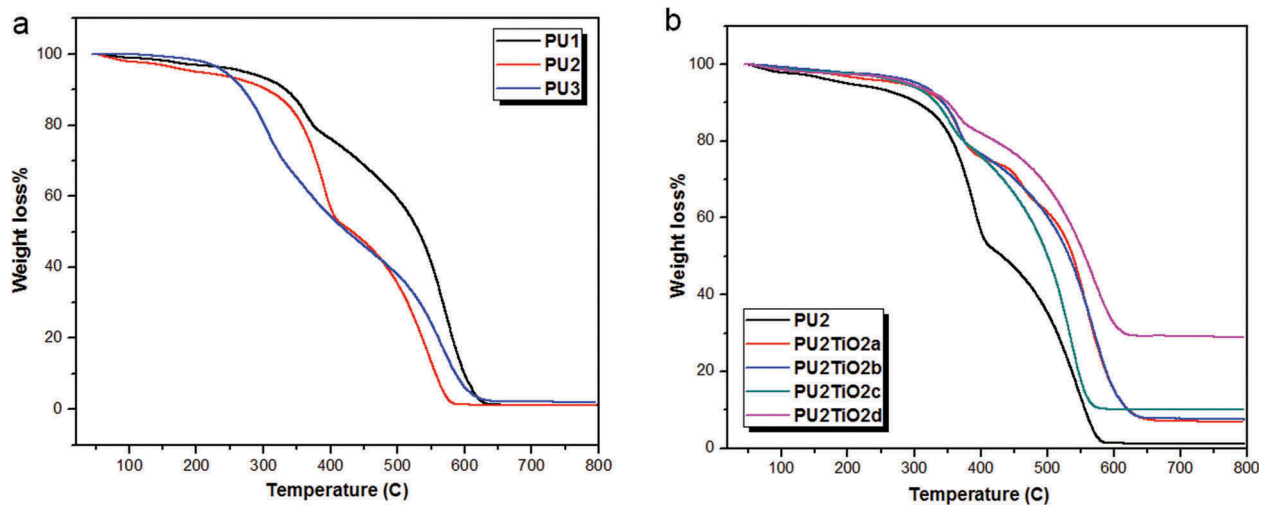


Figure 8. (a) TGA curves of  $\text{PU}_1$ ,  $\text{PU}_2$ ,  $\text{PU}_3$  in air at a heating rate of  $10^\circ\text{C}/\text{min}$ . (b) TGA curves of polyurea- $\text{TiO}_2$  nanocomposites  $\text{PU}_2$ ,  $\text{TiO}_2\text{a-d}$  in air at a heating rate of  $10^\circ\text{C}/\text{min}$ .



### 3.2. Polyurea-based TiO<sub>2</sub>nanocomposites fabrication

The same procedure was used to synthesise polyurea PU<sub>2</sub> using the solution polycondensation technique by first dissolving TiO<sub>2</sub> with different ratios (2%,5%,10%, and 20%) in dry pyridine and then dissolving one mole of M3 with one mole of 4,4'-diphenylmethane diisocyanate compound. The pyridine polymer and nanocomposites information are presented in Table 1. The polyurea and nanocomposite structures were confirmed by FTIR as presented in the experimental section. The IR spectra of PU<sub>2</sub>TiO<sub>2</sub>a–d show absorption bands at 3330 cm<sup>-1</sup>(NH of urea derivative) and 1660 cm<sup>-1</sup>(C = O of urea derivative), as shown in Figure 4(b).

The resulting polyurea derivatives and nanocomposites were characterised using XRD and TGA to determine the thermal stability of polyurea derivatives and nanocomposites and the influence of variable TiO<sub>2</sub> nanoparticles concentration on their thermal stability. The morphology exhibits features associated with agglomeration and concentration of TiO<sub>2</sub> nanoparticles on the polyurea surface as seen in SEM and TEM images.

The fabricated nanocomposites were characterised by XRD, SEM, TEM, and TGA. First, polyurea derivatives were measured as shown in Figure 5(a). PU<sub>1</sub> had four characteristic peaks at 2-theta values of 20.91°, 21.94°, 26.37°, and 42.8°, and d-space values of 4.5 Å, 4.2 Å, 3.51 Å, and 2.5 Å. PU<sub>2</sub> had four characteristic peaks at 2-theta values of 19.72°, 21.18°, 26.15°, and 41.18°, and

**Table 4.** TGA analyses for PU<sub>2</sub> and its related PU<sub>2</sub>TiO<sub>2</sub>a-d nanocomposites.

Code	IDT <sup>a</sup>	PDT <sub>max</sub> <sup>b</sup>	FDT <sup>a</sup>	Temperature (°C) for various percentage decompositions*				
				T <sub>10</sub>	T <sub>20</sub>	T <sub>30</sub>	T <sub>40</sub>	T <sub>50</sub>
PU <sub>2</sub>	363.41	567.9	612.3	332.9	374.1	441.8	496.7	531.1
PU <sub>2</sub> TiO <sub>2</sub> a	364.4	571.3	614.2	338.2	374.6	444.2	489.2	521.6
PU <sub>2</sub> TiO <sub>2</sub> b	366.34	587.5	622.3	343.2	374.9	451.6	501.6	532.9
PU <sub>2</sub> TiO <sub>2</sub> c	367.48	556.3	602.3	333.1	374.2	434.1	474.1	500.6
PU <sub>2</sub> TiO <sub>2</sub> d	368.25	596.2	650.2	350.2	421.4	491.9	530.1	556.6

<sup>a</sup>The values were determined by TG curves at heating rate of 10°C/min

<sup>b</sup>The values were determined by DTG.

**Table 5.** Antimicrobial and antifungal activity of tested polyurea derivatives PU<sub>1-3</sub> and its related nanocomposites PU<sub>2</sub>TiO<sub>2</sub>a-d.

POLYMER	S. AUREUS	B. SUBTILIS	P. AERUGINOSA	E. COLI	C. ALBICANS
PU <sub>1</sub>	3	–	2	–	–
PU <sub>2</sub>	2	2	3	2	3
PU <sub>3</sub>	–	–	2	–	2
PU <sub>2</sub> TiO <sub>2</sub> a	8	5	8	6	4
PU <sub>2</sub> TiO <sub>2</sub> b	9	8	10	7	6
PU <sub>2</sub> TiO <sub>2</sub> c	11	10	9	12	8
PU <sub>2</sub> TiO <sub>2</sub> d	12	10	12	14	10

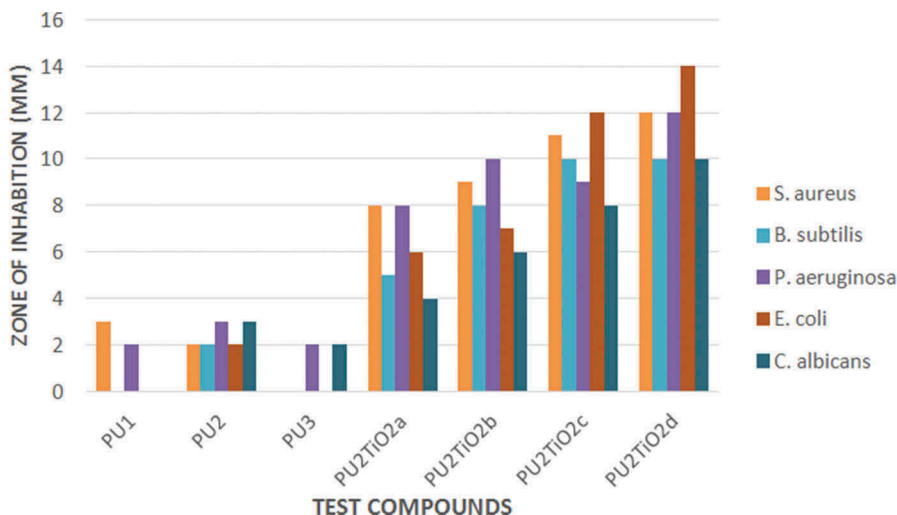


**Figure 9.** Antibacterial and antifungal activities of tested polyurea derivatives and polyurea-TiO<sub>2</sub> nanocomposites.

d-space values of 4.242 Å, 4.048, Å3.332 Å, and 2.11 Å. PU<sub>3</sub> had two characteristic peaks at 2-theta values of 19.72° and 37.42° with d-space values of 3.78 Å and 2.4 Å. PU<sub>3</sub> was crystalline or semi-crystalline, possibly because of the six methylene groups, which might be the result of increasing polyurea chain flexibility in adjacent chains [46]. Additionally, the presence of the high C = C band and C = O band, which represent polar groups arranged between the adjacent polyurea chains, could have caused the extended crystallinity [47]. The XRD patterns for polyurea-based TiO<sub>2</sub> nanocomposites with different percentages of TiO<sub>2</sub> nanoparticles (2, 5, 10, and 20%) were measured as shown in Figure 5(b). The XRD

patterns showed that polyurea with TiO<sub>2</sub> nanoparticles had characteristic peaks at 2-theta values of 25.25°, 36.96°, 37.93°, 38.61°, 48.1°, 53.89°, 55.30°, 63.2°, and 69.6°, and TiO<sub>2</sub> peak indices (101), (104), (200), (105), and (211) Compared to a standard card (00–002-0387), the TiO<sub>2</sub> nanoparticles peaks match those of anatase. Moreover, the XRD results for these nanocomposites also indicate a gradual decrease in the PU<sub>2</sub> related peaks as a result from the increase in the TiO<sub>2</sub> loading percent from PU<sub>2</sub>TiO<sub>2</sub>a to PU<sub>2</sub>TiO<sub>2</sub>d.

The morphology of selected samples PU<sub>2</sub>TiO<sub>2</sub>b and PU<sub>2</sub>TiO<sub>2</sub>d were examined as shown in Figure 6(a). At magnification X = 100,000, the PU<sub>2</sub>TiO<sub>2</sub>b surface was

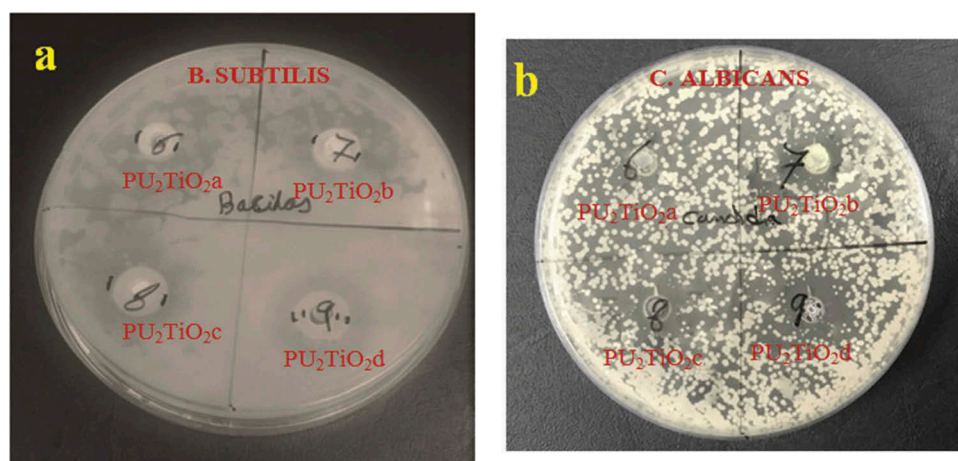


Figure 10. Antimicrobial activity images of tested polyurea-TiO<sub>2</sub> nanocomposites against *B. subtilis* and *C. Albicans*.

Table 6. Docking score and energies of PU<sub>1</sub>, PU<sub>2</sub>, and PU<sub>3</sub> with 5fsa receptor.

mseq	S	rmsd_refine	E_conf	E_place	E_refine	h_logD	h_logP	h_logS
PU <sub>1</sub>	-11.90	2.39	-127.14	-102.13	-66.30	8.70	9.25	-11.71
PU <sub>1</sub>	-11.89	2.82	-131.02	-105.91	-63.60	8.70	9.25	-11.71
PU <sub>1</sub>	-11.87	1.79	-123.67	-79.06	-67.66	8.70	9.25	-11.71
PU <sub>1</sub>	-11.71	2.92	-134.36	-83.77	-68.96	8.70	9.25	-11.71
PU <sub>1</sub>	-11.54	1.83	-95.81	-47.29	-64.98	8.70	9.25	-11.71
PU <sub>2</sub>	-12.92	3.98	-97.54	-84.27	-72.99	10.78	11.33	-13.71
PU <sub>2</sub>	-12.78	3.10	-117.60	-90.28	-79.61	10.78	11.33	-13.71
PU <sub>2</sub>	-12.75	2.59	-109.11	-57.11	-63.60	10.78	11.33	-13.71
PU <sub>2</sub>	-12.49	1.92	-127.03	-87.50	-73.70	10.78	11.33	-13.71
PU <sub>2</sub>	-12.43	1.91	-115.05	-111.26	-65.02	10.78	11.33	-13.71
PU <sub>3</sub>	-12.11	2.13	-132.83	-97.56	-70.86	7.81	8.37	-10.87
PU <sub>3</sub>	-11.86	1.88	-119.59	-116.25	-67.15	7.81	8.37	-10.87
PU <sub>3</sub>	-11.80	3.56	-123.73	-84.80	-61.64	7.81	8.37	-10.87
PU <sub>3</sub>	-11.70	2.08	-109.67	-139.36	-52.77	7.81	8.37	-10.87
PU <sub>3</sub>	-11.70	1.84	-106.54	-65.27	-52.11	7.81	8.37	-10.87

PU<sub>2</sub>TiO<sub>2</sub>c PU<sub>2</sub>TiO<sub>2</sub>d

Table 7. Distance and energy between PU<sub>1</sub>, PU<sub>2</sub>, and PU<sub>3</sub> with 5fsa receptor.

Product	Ligand	Receptor	Interaction	Distance	E (kcal/mol)
PU <sub>1</sub>	-	-	-	-	-
PU <sub>2</sub>	N 71	O SER 378 (A)	H-donor	3.29	-2.1
PU <sub>3</sub>	S 42	O SER 378 (A)	H-donor	3.68	-0.5
	N 43	SD MET 508 (A)	H-donor	4.07	-2.7
	5-ring	CD1 LEU 376 (A)	pi-H	3.86	-1.0

comprised of fibrous structures and the addition of 5 wt.% TiO<sub>2</sub> to the polymer caused agglomeration on the surface of the polymer. Additionally, in Figure 6(b), at magnification X = 13,000 in PU<sub>2</sub>TiO<sub>2</sub>d, the fibre morphology of polyurea and spherical morphology of 20 wt.% of TiO<sub>2</sub> nanoparticles showed excellent homogenous size distribution of TiO<sub>2</sub> nanoparticles on the polyurea surface.

The TEM image for PUTiO<sub>2</sub>d (TiO<sub>2</sub> nanoparticles 20%) in Figure 7 shows the spherical TiO<sub>2</sub> nanoparticles dispersed in polyurea (fibre shape) with homogenous size, shape, and distribution without any agglomeration or concentration in certain areas. TiO<sub>2</sub> nanoparticles are approximately 25 nm.

The thermographs of polyurea derivative samples are given in Figure 8(a), which shows the same decomposition curve for all samples with multi-step processes, starting with conformable removal of the (OH) group due to the removal of moisture content and/or entrapped solvents that cause weight loss; however, this step starts at room temperature and ends at approximately 160°C for PU<sub>1</sub>, PU<sub>2</sub>, and PU<sub>3</sub> with mass losses 0.338, 0.245, and 0.025 mg, respectively. The thermographs also show that polyurea derivatives decompose in two stages. The first stage is the partial decomposition of polymers, which starts at 160 C° and ends at 368°C, 345°C, and 337 C° for PU<sub>1</sub>, PU<sub>2</sub>, and PU<sub>3</sub>, with mass losses of 2.40, 3.261, and 3.50 mg, respectively. The second stage of decomposition starts at 350°C and ends at 612°C, 595°C, and 580°C for PU<sub>1</sub>, PU<sub>2</sub>, and PU<sub>3</sub>. The total mass loss of polyurea

derivatives shows higher stability for PU<sub>2</sub> than other polyurea derivatives with total mass loss at 800°C of 4.44 mg while PU<sub>1</sub> and PU<sub>3</sub> are 16.06 and 8.063 mg, respectively. Additionally, the TGA of polyurea–TiO<sub>2</sub> nanocomposite with different percentages of TiO<sub>2</sub>, as shown in Figure 8 (b), was performed to compare the thermal stability of each nanocomposite and explain the effect of TiO<sub>2</sub> nanoparticles on the thermal resistance of polyurea. The TGA curves for PU<sub>2</sub> and PU<sub>2</sub>TiO<sub>2</sub>a with different percentages of TiO<sub>2</sub> nanoparticles illustrate the effect of TiO<sub>2</sub> nanofiller on the thermal stability of polymers as shown in Figure 8 (b). The TGA data analysis shows the high thermal stability for PUTiO<sub>2</sub>d (20% TiO<sub>2</sub> nanofiller) with total mass loss of 71% compared to PUTiO<sub>2</sub>a, PUTiO<sub>2</sub>b, and PUTiO<sub>2</sub> c, which has losses of 94.66%, 94.54%, and 90.44%, respectively. The thermal properties are enhanced for all samples due to the high thermal resistance of the TiO<sub>2</sub> nanofiller. The initial decomposition temperature (IDT) at which the initial degradation may occur [48,49] was found to be in the range between 300°C and 560°C. T<sub>10</sub> was considered as the polymer decomposition temperature (PDT) with a range from 333°C to 350.2°C. Therefore, the data in Table 4 indicate the high thermal stability of PUTiO<sub>2</sub>a–d compared to individual polyurea. PDT<sub>max</sub> represents the maximum temperature at which the decomposition process occurs [49,50]. PDT<sub>max</sub> results show that all the polymers have similar PDT<sub>max</sub> values in the range from 531°C to 560°C. The final decomposition temperature (FDT) is the temperature at which the amount of degradation that

**Table 8.** Docking score and energies of PU<sub>1</sub>, PU<sub>2</sub>, and PU<sub>3</sub> with 1KZN receptor.

mseq	S	rmsd_refine	E_conf	E_place	E_refine	h_logD	h_logP	h_logS
PU <sub>1</sub>	-10.12	1.52	-135.34	-102.54	-60.59	8.70	9.25	-11.71
PU <sub>1</sub>	-9.61	2.42	-142.01	-105.79	-63.16	8.70	9.25	-11.71
PU <sub>1</sub>	-9.46	2.50	-140.00	-82.31	-59.95	8.70	9.25	-11.71
PU <sub>1</sub>	-9.43	3.01	-139.54	-78.94	-60.70	8.70	9.25	-11.71
PU <sub>1</sub>	-9.19	2.02	-142.39	-89.25	-59.09	8.70	9.25	-11.71
PU <sub>2</sub>	-10.38	2.21	-119.74	-70.35	-58.54	10.78	11.33	-13.71
PU <sub>2</sub>	-9.94	2.29	-127.41	-46.42	-63.84	10.78	11.33	-13.71
PU <sub>2</sub>	-9.82	2.14	-133.69	-73.17	-68.89	10.78	11.33	-13.71
PU <sub>2</sub>	-8.81	2.43	-126.65	-36.69	-51.48	10.78	11.33	-13.71
PU <sub>2</sub>	-8.69	1.94	-133.67	-87.72	-50.66	10.78	11.33	-13.71
PU <sub>3</sub>	-8.24	2.23	-134.24	-79.43	-47.01	7.81	8.37	-10.87
PU <sub>3</sub>	-8.17	3.93	-139.43	-60.48	-47.30	7.81	8.37	-10.87
PU <sub>3</sub>	-8.17	1.88	-133.60	-70.42	-49.44	7.81	8.37	-10.87
PU <sub>3</sub>	-8.06	2.49	-136.33	-55.69	-46.41	7.81	8.37	-10.87
PU <sub>3</sub>	-7.99	5.07	-138.08	-76.02	-54.55	7.81	8.37	-10.87

**Table 9.** 2D Docking structures and Distance between PU<sub>1</sub>, PU<sub>2</sub>, and PU<sub>3</sub> with 1KZN receptor.

Product	Ligand	Receptor	Interaction	Distance	E (kcal/mol)
PU <sub>1</sub>	–	–	–	–	–
PU <sub>2</sub>	N 97	O TYR 26 (A)	H-donor	3.01	-4.1
	N 48	NH1 ARG 136	(A) H-acceptor	3.09	-0.9
	6-ring	CD1 ILE 90 (A)	pi-H	4.24	-0.8
PU <sub>3</sub>	6-ring	CD PRO 79 (A)	pi-H	4.55	-0.8

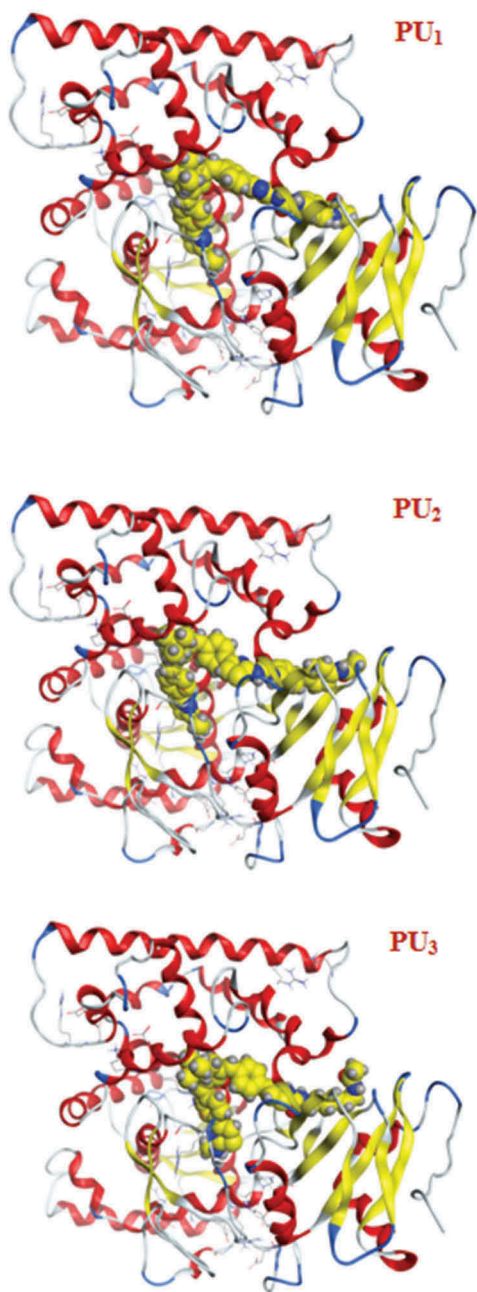


**Figure 11.** 3D Docking structures of PU<sub>1</sub>, PU<sub>2</sub>, and PU<sub>3</sub> with 5fsa receptor.

may occur is nearly completed [8,51]. The TG curves show that the FDT for all polymers is almost completed at around 600–650.2°C. By comparison, at the T<sub>40</sub> and T<sub>50</sub> values, the thermal stability increased with the increased percent of TiO<sub>2</sub> nanoparticles.

### 3.3. Antimicrobial Evaluation

The antimicrobial activity of the polyurea derivatives and TiO<sub>2</sub>-based nanocomposites was determined through the disk diffusion system with different

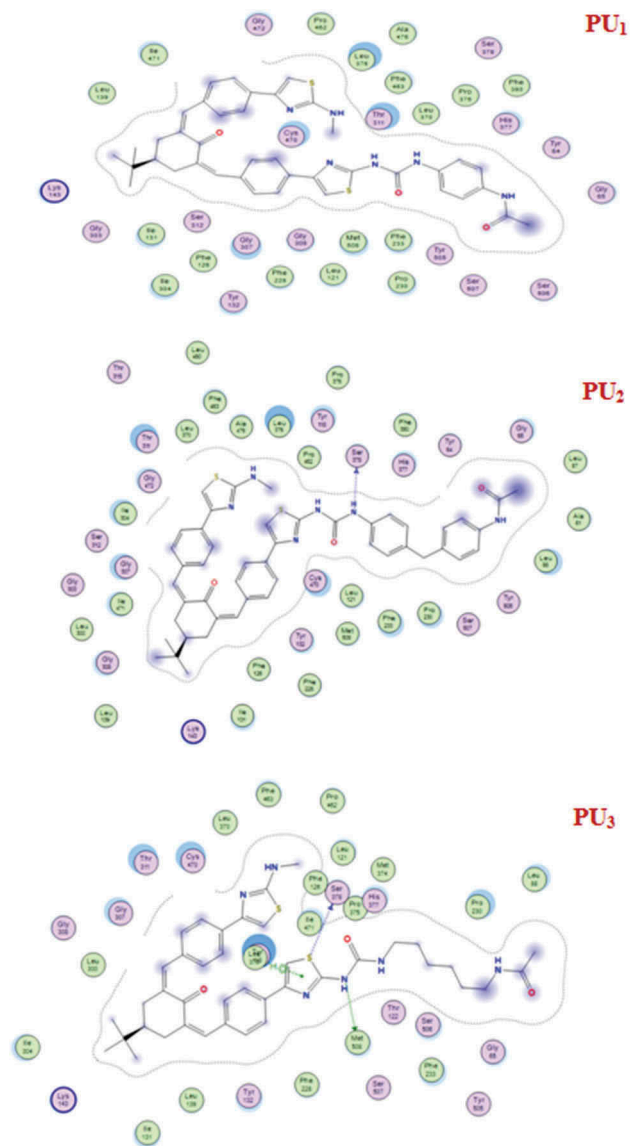


**Figure 12.** 2D Docking structures and Distance between PU<sub>1</sub>, PU<sub>2</sub>, and PU<sub>3</sub> with 5fsa receptor.

gram positives of *B. subtilis* and *S. aureus*, and gram negatives of *E. coli* and *P. aeruginosa* bacteria as well as the fungus *C. albicans* samples. The antimicrobial activity was evaluated by the inhibition zone diameters as presented in Figures 9 and 10 and Table 5. The tested polyurea derivatives showed activity against some of the microbial strains but the antibacterial activity against *B. subtilis*, *S. aureus*, *E. coli*, *P. aeruginosa*, and the fungus *C. albicans* was enhanced after addition TiO<sub>2</sub> nanoparticles. However, in some previous studies, the addition of TiO<sub>2</sub> to composites reduced bacterial attachment to the polymer surface [52–55]. But in most other cases it is reported as a good candidate which promotes the biological screening of materials [56–61]. The increase in added



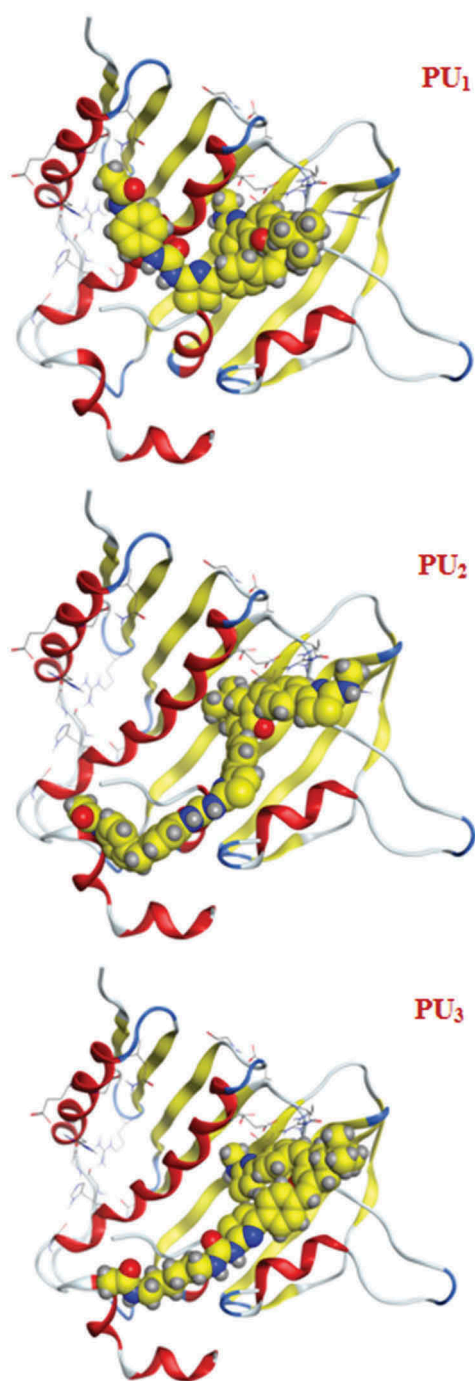


**Figure 13.** 3D Docking structures of PU<sub>1</sub>, PU<sub>2</sub>, and PU<sub>3</sub> with 5fsa receptor.

TiO<sub>2</sub> (2%, 5%, 10%, and 20%) showed increased antibacterial activity against all the microbial strains. The maximum antibacterial activity was observed against *E. coli*, with an inhibition zone of 14 mm for PU<sub>2</sub>TiO<sub>2</sub> d; therefore, the nanocomposites were more active against *E. coli* than other types of bacteria, so it is clear that with the increase in TiO<sub>2</sub> concentration, the zone of inhibition increased.

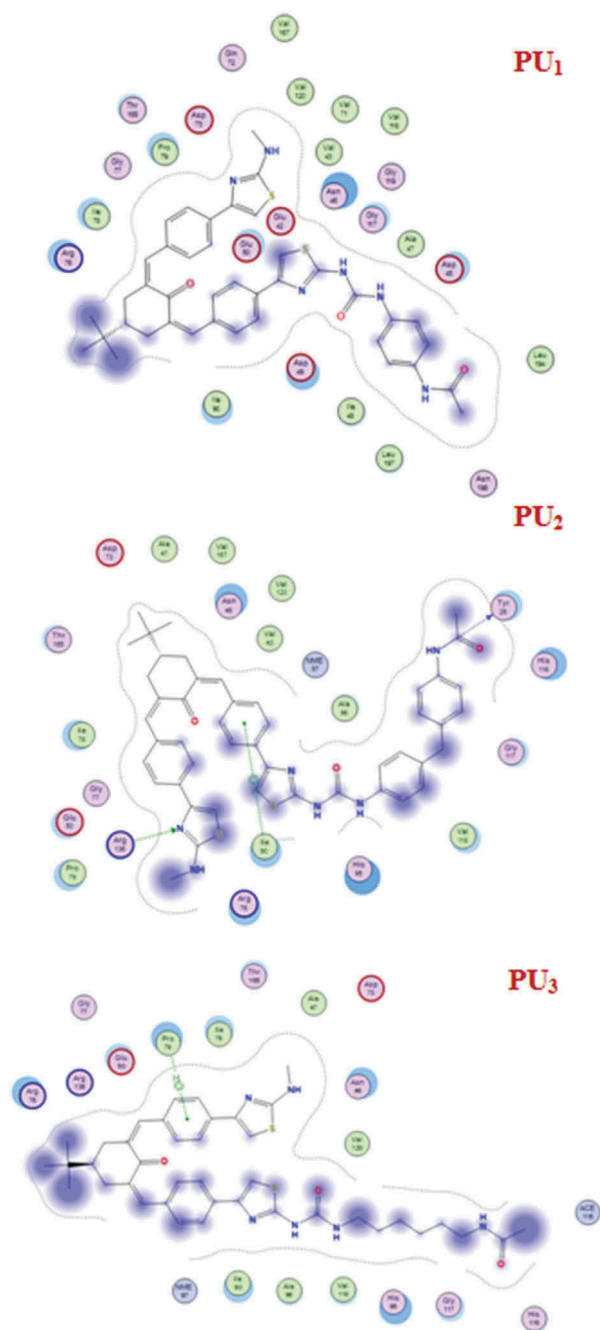


**Figure 14.** Distance and energy between PU<sub>1</sub>, PU<sub>2</sub>, and PU<sub>3</sub> with 1KZN receptor.

### 3.4. Molecular docking study

The docking studies have been applied to PU<sub>1</sub>, PU<sub>2</sub>, and PU<sub>3</sub> compounds against the '5FSA' protein [62,63] and '1KZN' [64,65] to highlight the possible acting functional groups. 5FSA is the sterol 14- $\alpha$  demethylase (cyp51), which is a cytochrome P450 enzyme that is employed for the biosynthesis of sterols in cells and is the major target of clinical drugs in fungi [62]. 1KZN is a code for the 24 kDa gyrase fragment; DNA gyrase is a primary protein

involved in replication and transcription of bacterial circular DNA [64]. Many antibacterial drugs are known to target DNA gyrase, inducing bacterial death [64]; a similar docking study was undertaken on the clinically approved drugs Gentamycin for the 1KZN protein and Fluconazole for 5FSA. The docking of 1KZN against the compounds and the antibacterial reference suggest an increase in the docking score of PU<sub>2</sub> over PU<sub>1</sub> and PU<sub>3</sub> (Table 6–9). The docking score of PU<sub>2</sub> compared to PU<sub>1</sub> and PU<sub>3</sub> (Figures 11–14) can be attributed to both electronic interaction and its orientation inside the protein sites. Similarly, the docking study of 5FSA against the compounds and the antifungal reference ‘Fluconazole’ revealed similar observations. The docking scores are in good agreement with the antimicrobial effectiveness of the compounds against *E. coli* and the antifungal capacities of the compounds against *S. aureus*, *B. subtilis*, and *P. aeruginosa*.

#### 4. Conclusions

A series of polyurea derivatives and polyurea–TiO<sub>2</sub> nanocomposites were successfully synthesised in pyridine using the polycondensation technique. The structure was confirmed by FTIR, and characterised using XRD, TGA, and SEM. TGA showed a high thermal stability for polyurea–TiO<sub>2</sub> nanocomposites with the increase in TiO<sub>2</sub> nanoparticles. The synthesised TiO<sub>2</sub> nanocomposites emerged as good antimicrobial agents. TEM images for PU<sub>2</sub>TiO<sub>2</sub>d showed the spherical TiO<sub>2</sub> nanoparticles dispersed into polyurea (fibre shape), also SEM images for PU<sub>2</sub>TiO<sub>2</sub>b and PU<sub>2</sub>TiO<sub>2</sub>d showed a fibrous polymer structure with spherical morphology for the TiO<sub>2</sub>. The polyurea derivatives showed slight antibacterial activity and after adding TiO<sub>2</sub> nanoparticles showed activity against all the microbial strains; the activity increased with the increase in TiO<sub>2</sub> present.

#### Disclosure statement

No potential conflict of interest was reported by the authors.

#### References

- [1] Chantarasiri N, Chulamanee C, Mananunsap T, et al. Thermally stable metal-containing polyureas from hexadentate Schiff base metal complexes and diisocyanates. *Polym Degrad Stab.* 2004;86(3):505–513.
- [2] Mallakpour S, Raheno H. Synthesis and characterization of new polyureas based on 4-(4'-aminophenyl) urazole and various diisocyanates. *J Appl Polym Sci.* 2003;89(10):2692–2700.
- [3] Lin JK, Yuki Y, Kunisada H, et al. Synthesis and characterization of new aromatic polyamides, polyimides, and polyureas containing 1, 3, 5-triazine rings. *J Appl Polym Sci.* 1990;40(11-12):2113–2122.
- [4] Melissaris AP, Mikroyannidis JA. Phosphorus-containing crosslinkable polymers for fire- and heat-resistant applications. *Eur Polym J.* 1989;25(3):275–280.
- [5] Miyamoto M, Takashima Y, Kimura Y. Preparation of novel thermally stable polyurea by the cationic ring-opening isomerization polymerization of polycyclic pseudourea. *Macromolecules.* 1998;31(20):6822–6827.
- [6] Matsuda H, Takechi S. Syntheses and properties of polyureas from divalent metal salts of p-aminobenzoic acid, diamine, and diisocyanate. *J Polym Sci A Polym Chem.* 1990;28(7):1895–1908.
- [7] Qiu W, Zeng W, Zhang X, et al. Preparation and characterization of polyureas from divalent metal (Ba, Sr, Pb, Zn) salts of sulfanilic acid. *J Appl Polym Sci.* 1993;49(3):405–415.
- [8] Aly K, Hussein M. Synthesis, characterization and corrosion inhibitive properties of new thiazole based polyamides containing diarylidencyclohexanone moiety. *Chin J Polym Sci.* 2015;33(1):1–13.
- [9] Lagrenee M, Mernari B, Bouanis M, et al. Study of the mechanism and inhibiting efficiency of 3, 5-bis (4-methylthiophenyl)-4H-1, 2, 4-triazole on mild steel corrosion in acidic media. *Corros Sci.* 2002;44(3):573–588.
- [10] Bentiss F, Lagrenee M, Traisnel M, et al. The corrosion inhibition of mild steel in acidic media by a new triazole derivative. *Corros Sci.* 1999;41(4):789–803.
- [11] Lukovits I, Kalman E, Palinkas G. Nonlinear group-contribution models of corrosion inhibition. *Corrosion.* 1995;51(3):201–205.
- [12] Yao B, Wang G, Ye J, et al. Corrosion inhibition of carbon steel by polyaniline nanofibers. *Mater Lett.* 2008;62(12–13):1775–1778.
- [13] Sathiyarayanan S, Jeyaprabha C, Venkatachari G. Influence of metal cations on the inhibitive effect of polyaniline for iron in 0.5 M H<sub>2</sub>SO<sub>4</sub>. *Mater Chem Phys.* 2008;107(2–3):350–355.
- [14] Kilmartin PA, Trier L, Wright GA. Corrosion inhibition of polyaniline and poly (o-methoxyaniline) on stainless steels. *Synth Met.* 2002;131(1–3):99–109.
- [15] Aly KI, Abbady MA, Mahgoub SA, et al. New Polymer Synthesis Part 14. Synthesis and properties of some new polyketo-amine polymers containing cycloalkanone moieties in the main chain. *J Polym Int.* 2002;51(2):125–133.
- [16] Abbady MA, Aly KI, Mahgoub SA, et al. New polymer synthesis part 15. Synthesis and characterization of new polyketoamine polymers containing ether and thioether linkage in the main chain. *J Polym Int.* 2005;54(11):1512–1523.
- [17] Hussein MA, Abdel-Rahman MA, Geies AA. New hetero-aromatic polyazomethines containing naphthyridine moieties: synthesis, characterization, and biological screening. *J Appl Polym Sci.* 2012;126(1):2–12.
- [18] Aly KI, Abbady MA, Mahgoub SA, et al. New polymer syntheses 44. Synthesis, characterization and corrosion inhibition behavior of new polyurea derivatives based on diaryl ether in the polymers backbone. *J Appl Polym Sci.* 2009;112(2):620–628.
- [19] Aly KI, Abbady MA, Mahgoub SA, et al. Liquid crystalline polymers IX main chain thermotropic poly (azomethine –

- ether) containing thiazole moiety linked with polymethylene spacers. *J Express Polym Lett.* **2007**;1(4):197–207.
- [20] Aly KI, Abdel Rahman MA, Hussein MA. Synthesis and characterization of new polyamides of diarylidene-cycloalkanone moieties containing Azo groups in the polymers main chain. *Int J Polym Mater.* **2010**;59(8):553–569.
- [21] Aly KI, Hussein MA. New polymer syntheses part 45. Corrosion inhibition behavior of novel polyurea derivatives based on diarylidene-cycloalkanone moieties in the polymers backbone. *J Polym Res.* **2010**;17(5):607–620.
- [22] Hussein MA, Asiri AA, Aly KI. New polyamides and polyoxazoles containing diphenyl ether in the polymers backbone. *Int J Polym Mater.* **2012**;61(2):154–175.
- [23] Hussein MA, Asiri AM. Organometallic ferrocene- and phosphorus-containing polymers: synthesis and characterization. *Des Monomers Polym.* **2012**;15(3):207–251.
- [24] Hussein MA, Marwany H, Alamry KA, et al. Surface selectivity competition of newly synthesized polyarylidene (keto-amine)s polymers toward different metal ions. *J Appl Polym Sci.* **2014**;131(19):40873 (1–10).
- [25] Abu-Zied BM, Hussein MA, Asiri AM. Development and characterization of the composites based on mesoporous MCM-41 and polyethylene glycol and their properties. *Composites.* **2014**;58:185–192.
- [26] Hussein MA, Abu-Zied BM, Asiri AM. Preparation, characterization, and electrical properties of ZSM-5/PEG composite particles. *Polym Composites.* **2014**;35(6):1160–1168.
- [27] Gabal MA, Hussein MA, Hermas A-EA, et al. Electrical conductivity of polyaniline-Mn<sub>0.8</sub>Zn<sub>0.2</sub>Fe<sub>2</sub>O<sub>4</sub> nano-composites. *Int J Electrochem Sci.* **2016**;11:4526–4538.
- [28] Alenazi NA, Hussein MA, Alamry KA, et al. Modified polyether-sulfone membrane: A mini review. *Des Monomers Polym.* **2017**;20(1):532–546.
- [29] Rahman MM, Hussein MA, Alamry KA, et al. Polyaniline/graphene/carbon nanotubes nanocomposites for sensing environmentally hazardous 4-aminophenol. *Nano Struct Nano-Objects.* **2018**;15:63–74.
- [30] Hussein MA, El-Shishtawy RM, Obaid AY. The impact of graphene nano-plates on the behavior of novel conducting polyazomethine nanocomposites. *RSC Adv.* **2017**;7:9998–10008.
- [31] Hussein MA, El-Shishtawy RM, Obaid AY, et al. Influence of single-walled carbon nanotubes on the performance of poly(azomethine-ether) composite materials. *Polym-Plast Technol Eng.* **2018**;57(11):1150–1163.
- [32] Patel JP, Xiang ZG, Hsu SL, et al. Path to achieving molecular dispersion in a dense reactive mixture. *J Polym Sci B Polym Phys.* **2015**;53:1519–1526.
- [33] Patel JP, Deshmukh S, Zhao C, et al. An analysis of the role of nonreactive plasticizers in the cross-linking reactions of a rigid resin. *J Polym Sci B Polym Phys.* **2017**;55:206–213.
- [34] Patel JP, Zhao CX, Deshmukh S, et al. An analysis of the role of reactive plasticizers in the cross-linking reactions of a rigid resin. *Polymer.* **2016**;107:12–18.
- [35] Patel JP, Xiang ZG, Hsu SL, et al. Characterization of the cross-linking reaction in high performance adhesives. *Int J Adhes Adhes.* **2017**;78:256–262.
- [36] Patel JP, Hsu SL. Development of low field NMR technique for analyzing segmental mobility of cross-linked polymers. *J Polym Sci B Polym Phys.* **2018**;56:639–642.
- [37] Aly KI, Al-Muaiikel NS, Abdel-Rahman MA, et al. Liquid crystalline polymers XVI. Thermotropic liquid crystalline copoly (arylidene-ether)/TiO<sub>2</sub> nanocomposites: synthesis, characterisation and applications. *Liq Cryst.* **2019**;46(11):1734–1746.
- [38] Ge B, Wang F, Sjölund-Karlsson M, et al. Antimicrobial resistance in campylobacter: susceptibility testing methods and resistance trends. *J Microbiol Methods.* **2013**;95(1):57–67.
- [39] Abdellattif MH, Hussien MA, Alzahrani E. New approaches of 4-aryl-2-hydrazinethiazole derivatives synthesis, molecular docking and biological evaluations. *IJPSR.* **2018**;9:5060–5078.
- [40] Al-Khathami ND, Al-Rashdi KS, Babgi BA, et al. Spectroscopic and biological properties of platinum complexes derived from 2-pyridyl Schiff bases. *J. Saudi Chem. Soc.* **2019**; 23: 903–915.
- [41] Mashat KH, Babgi BA, Hussien MA, et al. Synthesis, structures, DNA-binding and anticancer activities of some copper(I)-phosphine complexes. *Polyhedron.* **2019**;158:164–172.
- [42] Al-Muaiikel NS, Aly KI, Hussein MA. Synthesis, characterization and antimicrobial properties of new poly (ether-ketone) s and copoly (ether-ketone)s containing diarylidene-cycloalkanone moieties in the main chain. *J Appl Polym Sci.* **2008**;108(5):3138–3147.
- [43] Baik YS, Cheong WJ. Determination of molecular weight distribution and average molecular weights of oligosaccharides by HPLC with a common C18 phase and a mobile phase with high water content. *Bull Korean Chem Soc.* **2007**;28(5):847–850.
- [44] García-Lopera R, Codoñer A, Bañó MC, et al. Size-exclusion chromatographic determination of polymer molar mass averages using a fractal calibration. *J Chromatogr Sci.* **2005**;43:1–9.
- [45] JANCO M, SYKORA D, SVEC F, et al. Rapid determination of molecular parameters of synthetic polymers by precipitation/redissolution high-performance liquid chromatography using “molded” monolithic column. *J Polym Sci.* **2000**;38:2767–2778.
- [46] C H L, Chang TC. Studies on thermotropic liquid crystalline polymers—part II. Synthesis and properties of poly (azomethine-ether). *Eur Polym J.* **1991**;27(1):35–39.
- [47] Mandelkern L. *Crystallization of polymers.* New York: McGraw-Hill; **1964**.
- [48] Rahman MM, Hussein MA, Aly KI, et al. Thermally stable hybrid polyarylidene(azomethine-ether)s polymers (paap): an ultrasensitive arsenic(III) sensor approach. *Des Monomers Polym.* **2018**;21(1):82–98.
- [49] Hussein MA. The role of mixed graphene/carbon nanotubes on the coating performance of G/CNTs/epoxy resin nanocomposites. *Int J Electrochem Sci.* **2016**;11:7644–7659.
- [50] Hussein MA, Abu-Zied BM, Asiri AM. Fabrication of EPYR/GNP/MWCNT carbon-based composite materials for promoted epoxy coating performance. *RSC Adv.* **2018**;8:23555–23566.

- [51] Hussein MA. Eco-friendly polythiophene (keto-amine)s based on cyclopentanone moiety for environmental remediation. *J Polym Environ.* 2018;26(3):1194–1205.
- [52] Høiby N, Ciofu O, Johansen HK, et al. The clinical impact of bacterial biofilms. *Int J Oral Sci.* 2011;3(2):55–65.
- [53] Hengzhuang W, Wu H, Ciofu O, et al. Pharmacokinetics/pharmacodynamics of colistin and imipenem on mucoid and nonmucoid *Pseudomonas aeruginosa* biofilms. *Antimicrob Agents Chemother.* 2011;55:4469–4474.
- [54] Hengzhuang W, Wu H, Ciofu O, et al. In vivo pharmacokinetics/pharmacodynamics of colistin and imipenem in *pseudomonas aeruginosa* biofilm infection. *Antimicrob Agents Chemother.* 2012;56:2683–2690.
- [55] Høiby N, Bjarnsholt T, Givskov M, et al. Antibiotic resistance of bacterial biofilms. *Int J Antimicrob Agents.* 2010;35:322–332.
- [56] Rajh T, Dimitrijevic NM, Bissonnette M, et al. Titanium dioxide in the service of the biomedical revolution. *Chem Rev.* 2014;114(19):10177–10216.
- [57] Zhiyuan L, Shuili Y, Heedeung P, et al. Impact of titanium dioxide nanoparticles on the bacterial communities of biological activated carbon filter intended for drinking water treatment. *Environ Sci Pollut Res.* 2016;23:15574–15583.
- [58] Ahmadi R, Tanomand A, Kazeminava F, et al. Fabrication and characterization of a titanium dioxide (TiO<sub>2</sub>) nanoparticles reinforced bio-nanocomposite containing *Miswak (Salvadora persica L.)* extract – the antimicrobial, thermo-physical and barrier properties. *Int J Nanomedicine.* 2019;14:3439–3454.
- [59] Zafar N, Uzair B, Niazi MBK, et al. Fabrication & characterization of chitosan coated biologically synthesized TiO<sub>2</sub> nanoparticles against PDR *E. coli* of veterinary origin. *Adv Polym Technol.* 2020;8456024:1–13.
- [60] Abbas WA, Abdullah IH, Ali BA, et al. Recent advances in the use of TiO<sub>2</sub> nanotube powder in biological, environmental, and energy applications. *Nanoscale Adv.* 2019;1(8):2801–2816.
- [61] Mallakpour S, Zeraatpisheh F, Sabzalian MR. Sonochemical-assisted fabrication of biologically active chiral poly(ester-imide)/TiO<sub>2</sub>bionanocomposites derived from L-methionine and L-tyrosine amino acids. *Express Polym Lett.* 2011;5(9):825–837.
- [62] Kaur H, Gahlawat S, Singh J, et al. Molecular docking study of active diazenyl scaffolds as inhibitors of essential targets towards antimicrobial drug discovery. *Curr Drug Targets.* 2019;20(15):1587–1602.
- [63] Hargrove TY, Friggeri L, Wawrzak Z, et al. Structural analyses of candida albicans sterol 14 $\alpha$ -demethylase complexed with azole drugs address the molecular basis of azole-mediated inhibition of fungal sterol biosynthesis. *J Biol Chem.* 2017;292:6728–6743.
- [64] Gullapelli K, Brahmeshwari G, Ravichander M, et al. Synthesis, antibacterial and molecular docking studies of new benzimidazole derivatives. *Egypt J Basic Appl Sci.* 2017;4(4):303–309.
- [65] Lafitte D, Lamour V, Tsvetkov PO, et al. DNA gyrase interaction with coumarin-based inhibitors: the role of the hydroxybenzoate isopentenyl moiety and the 5'-methyl group of the noviose. *Biochemistry.* 2002;41:7217–7223.